Magnetic Anisotropy and Slow Relaxation of Magnetisation in Double Salts Containing Four- and Six-Coordinate Cobalt(II) Complex Ions

Jana Juráková,[ab] Vinicius Tadeu Santana,[a] Ján Pavlik,[b] Ján Moncoľ,[b] Ivan Nemec,[ac] Miguel Clemente-León,[d] Kuppusamy Senthil Kumar,[e] Mario Ruben,[e] Erik Čižmár,[f] Ivan Šalitroš[ab*]

a) Central European Institute of Technology, Brno University of Technology, Purkyňova 123, 61200 Brno Czech Republic
b) Department of Inorganic Chemistry, Faculty of Chemical and Food Technology, Slovak University of Technology in Bratislava. Bratislava SK-81237, Slovakia. *e-mail: ivan.salitros@stuba.sk
c) Department of Inorganic Chemistry, Faculty of Science, Palacký University, 17. listopadu 12, 771 46 Olomouc, Czech Republic
d) Instituto de Ciencia Molecular (ICMol), Universidad de Valencia, Catedrático José Beltrán 2, 46980 Paterna, Spain
e) Institute of Nanotechnology (INT), Karlsruhe Institute of Technology (KIT), Hermann-von-Helmholtz-Platz 1, 76344 Eggenstein-Leopoldshafen, Germany.
f) Institute of Physics, Faculty of Science, P.J. Šafárik University Park Angelinum 9, 04154 Košice, Slovakia

Contents

S1 Magneto-structural properties in $[Co(L)_2][Co(X_{ps})_4]$ coordination compounds

Table S1 Overview of magnetic parameters observed in series ionic coordination compounds $[Co(L)_2][Co(X_{ps})_4]$ with tridentate N-donor ligands and pseudohalide anions

	Structural parameters	**Magnetic anisotropy parameters**	**SRM parameters**
Compound **1** $[Co(L1)_2][Co(NCS)_4]\cdot 0.5CH_3CN$ (this work)	Σ=136° S(OC-6)=4.94	D_{Oct}/cm^{-1}= 70.0[m] (40.8)[a] E/D_{Oct}= 0[m] (0.11)[a]	No maximum in χ'' up to 10 kHz
	τ_4=0.97 S(T-4)=0.03	D_{Tet}/cm^{-1}= -6.6[m] (-3.2)[a] E/D_{Tet}= 0[m] (0.14)[a]	
Compound **2** $[Co(L1)_2][Co(NCO)_4]$ (this work)	Σ=133° (Co1A), 137° (Co2A), S(OC-6) = 4.25(Co1A), 4.75(Co1B)	D_{Oct}/cm^{-1}= 36.8[m] (52.0)[a] E/D_{Oct}= 0[m] (0.06)[a]	τ = 92(2) μs at 2.0 K; U_{eff}=8.4 K
	τ_4=0.93 (Co2A); 0.89 (Co2B). S(T-4)=0.16 (Co2A); 0.47 (Co2B).	D_{Tet}/cm^{-1}= 7.7[m] (6.0)[a] E/D_{Tet}= 0[m] (0.2)[a]	
Compound **3** $[Co(L2)_2][Co(NCO)_4]$ (this work)	Σ=124° S(OC-6)= 4.00	D_{Oct}/cm^{-1}= 94.5[m] (57.1)[a] E/D_{Oct}= 0[m] (0.04)[a]	No maximum in χ'' up to 10kHz
	τ_4=0.97 S(T-4)=0.06	D_{Tet}/cm^{-1}= -7.5[m] (-3.5)[a] E/D_{Tet}= 0[m] (0.08)[a]	
Compound **4** $[Co(L3)_2][Co(NCO)_4]\cdot 2CH_3CN$ (this work)	Σ=131° S(OC-6)= 4.46	D_{Oct}/cm^{-1}= 49.2[m] (57.7)[a] E/D_{Oct}= 0[m] (0.01)[a]	No maximum in χ'' up to 10kHz
	τ_4=0.97 S(T-4)=0.04	D_{Tet}/cm^{-1}= 3.8[m] (2.2)[a] E/D_{Tet}= 0[m] (0.29)[a]	
$[Co(bbp)_2][Co(NCS)_4]$[1]	Σ=130° S(OC-6)=4.72	D_{Oct}/cm^{-1}= 39.0[m] (47)[a] E/D_{Oct}= 0.09[m] (0.09)[a]	No maximum in χ'' up to 1kHz
	τ_4=0.93 S(T-4)=0.05	D_{Tet}/cm^{-1}= 0[m] (-1.3)[a] E/D_{Tet}= 0[m] (0.2)[a]	
$[Co(mpyr\text{-}dtpy)_2][Co(NCS)_4]$[2]	Σ=132° S(OC-6)=4.6	$\Delta_{ax,Oct}/cm^{-1}$= −1200[GF]	τ=125 μs at 1.8 K
	τ_4=0.93 S(T-4)=0.26	D_{Tet}/cm^{-1}= -3.1[m]	
$[Co(brphterpy)_2][Co(NCS)_4]$[3]	Σ=106° S(OC-6)=2.71	$[Co(brphterpy)_2]^{2+}$ cation exhibits the above room temperature SCO.	τ=12.4 ms at 1.8 K U_{eff}=11.6 K
	τ_4=0.94 S(T-4)=0.20	D_{Tet}/cm^{-1}= 7.55[m] E/D_{Tet}= 0.01[m]	
$[Co(BTP)_2][Co(NCS)_4]$[4]	Σ=99.2° S(OC-6)=2.9	Compound is HS, analysis of DC magnetic data is not reported	AC data not reported
	τ_4=0.93 S(T-4)= 0.27		
$[Co((4\text{-}terpyridone)_2][Co(NCS)_4]$[5]	Σ=65.4° S(OC-6)=1.3 τ_4=0.92 S(T-4)= 0.26	Compound is HS, analysis of DC magnetic data is not reported	AC data not reported
$[Co(tppz)_2][Co(NCS)_4]$[6]	Σ=96.2° S(OC-6)= 2.31	$[Co(tppz)_2]^{2+}$ cation exhibits the above room temperature SCO.	AC data not reported
	τ_4=0.96 S(T-4)= 0.10	D_{Tet}/cm^{-1}= 3.80[m] E/D_{Tet}= 0	
$[Co(tppz)_2][Co(NCO)_4]$[6]	Σ=88.8° S(OC-6)=2.21	$[Co(tppz)_2]^{2+}$ cation exhibits the above room temperature SCO.	No maximum in χ'' up to 1kHz U_{eff}=11.7 cm^{-1}

	τ_4=0.95 *S*(T-4)=0.18	D_{Tet}/cm^{-1}= 4.30^{m} E/D_{Tet}= 0	
[Co(bdmpzpy)$_2$][Co(N$_3$)$_4$][7]	Σ=41° *S*(OC-6)=0.4 τ_4=0.95 *S*(T-4)=0.12	Magnetic investigation was not reported	
[Co(bdmpzpy)$_2$][Co(NCS)$_4$][7]	Σ=37° *S*(OC-6)=0.8 τ_4=0.95 *S*(T-4)=0.38 and 0.12	Magnetic investigation was not reported	

bbp=2,6-bis(1*H*-benzoimidazol-2- yl)pyridine; ***mpyr-dtpy***=4–(N–methyl–pyrrol–2–yl)–2,6–di(thiazol–2–yl)pyridine; ***brphterpy***=4′-(4-(pyridin-4-yl)phenyl)-[2,2′:6′,2″]terpyridine; **BTP**=2,6-Bis(5,6-dialkyl-1,2,4-triazin-3-yl)-pyridine; **4-terpyridone**=2,6-bis(2-pyridyl)- 4(1*H*)-pyridone; **tppz**=2,3,5,6-tetrakis-(2-pyridyl)pyrazine; **bdmpzpy**=2,6-bis[(3,5-dimethyl-pyrazol-1H-yl)-methyl]pyridine

[m]magnetic data analysis of experimental data; [a]*ab initio* calculations; [GF]parameters of Grifith-Figgis Hamiltonian

S2 Experimental section

S 2.1Materials and methods

Acetonitrile p.a., $CoCl_2$, KNCO and $Co(NCS)_2$ were purchased from Sigma-Aldrich or Mikrochem, s.r.o and used as received without any further purification. Elemental analysis of carbon, hydrogen and nitrogen was carried out by EA CHNS(O) Flash 1112 machine. FT-IR spectra of the reported compounds were measured on Nicolet 5700 spectrometer in the interval from 4000 to 400 cm^{-1} (ATR technique). The UV-VIS spectra were measured on Specord 200 spectrophotometer in the range of 800–190 nm. The starting compound 2,6-bis(1*H*-benzimidazole-2-yl)pyridine for synthesis of L1-L3 was prepared by condensation of o-phenylenediamine and pyridine-2,6-dicarboxylic acid following a documented protocol.[8] The synthesis of ligands L2 (2,6-bis(1-octyl-1*H*-benzimidazol-2-yl)pyridine) and L3 (2,6-bis(1-dodecyl-1*H*-benzimidazol-2-yl)pyridine) was reported previous.[9]

S 2.2 Synthesis

Synthesis of 2,6-bis(1-hexyl-1H-benzimidazol-2-yl)-pyridine (L1)

The ligand L1 was synthesized using 2,6-bis(1*H*-benzimidazol-2-yl)pyridine as the starting reactant. The reaction was performed in a 50-ml round-bottom flask charged with 0.5 g (1.6 mmol, 1 eq) of 2,6-bis(2-benzimidazolyl)pyridine dissolved in 10 ml of DMF. Then, 1.1 g (8.0 mmol, 5 eq) of K_2CO_3 was added to the solution, and the suspension was stirred for 2 hours at 70°C. Next, 0.66 ml (4.0 mmol, 2.5 eq) of 1-bromohexane was added dropwise over the stirring suspension. The reaction mixture was refluxed at 120 °C for 36 hours and then allowed to cool to room temperature. Finally, the solvent was removed by vacuum distillation, and the residue was treated with distilled water (50 ml) and extracted with CH_2Cl_2 (3 x 100 ml). The dichloromethane was removed using a rotary evaporator, and the oily residue was separated using column chromatography on silica gel with ethyl acetate/petroleum ether (4:1) as the eluent. The main product L1 was isolated as the fraction (R_f = 0.55) in a yield of 73 % (0.56 g, 1.17 mmol) as an orange, sticky and oily liquid. M_r = 479.7. ^{1}H NMR (700 MHz, d_6-DMSO, 25 °C, δ/ppm): 8.30 (d, *J* = 7.9 Hz, 2H), 8.23 (d, *J* = 7.5 Hz, 1H), 7.76 (d, *J* = 8.0 Hz, 2H), 7.70 (d, *J* = 8.1 Hz, 2H), 7.34 (t, *J* = 7.5 Hz, 2H), 7.29 (t, *J* = 7.5 Hz, 2H), 4.73 (t, *J* = 7.2 Hz, 4H), 1.64 (dd, *J* = 14.3, 7.2 Hz, 4H), 1.01 (dd, *J* = 13.8, 6.8 Hz, 4H), 0.96 – 0.84 (m, 8H), 0.51 (t, *J* = 6.8 Hz, 6H). ^{13}C NMR (176 MHz, d_6-DMSO, 25 °C, δ/ppm): 149.65, 149.60, 142.44, 138.80, 136.06, 125.24, 123.29, 122.41, 119.72, 111.09, 44.11, 30.42, 29.43, 25.52, 21.81, 13.49.

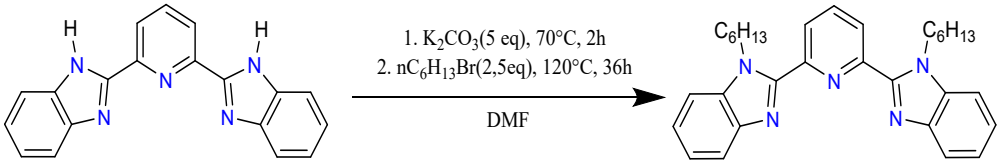

Figure S1 Synthesis of ligand L1.

*Synthesis of complexes **1** [Co(L1)$_2$][Co(NCO)$_4$], **3** [Co(L2)$_2$][Co(NCO)$_4$] and **4** [Co(L3)$_2$][Co(NCO)$_4$]·2CH$_3$CN*

An aqueous solution (5 ml) of $CoCl_2$ (65 mg, 0.5 mmol, 1 eq.) and KNCO (81 mg, 1.0 mmol, 2 eq.) was added into the acetonitrile solution (20 ml) of ligand **L1** (239 mg, 0.5 mmol, 1 eq), **L2** (268 mg, 0.5 mmol, 1 eq) or **L3** (324 mg, 0.5 mmol, 1 eq), respectively. The resulting mixture was refluxed at 80°C for next 45 minutes, filtered and the solution was set for controlled crystallisation at room temperature. Green block crystals suitable for X-ray diffraction were collected after a few days.

Complex **1** $[Co(L1)_2][Co(NCO)_4]$: Yield 43% (274 mg, 0.22 mmol). Elemental analysis for $C_{66}H_{74}Co_2N_{14}O_4$ (M_w = 1245.25 g mol^{-1}) found % (expected %): C 62.83 (63.66); N 14.92 (14.75); H 5.72 (5.99). FT−IR (ATR, $\tilde{\nu}_{max}$/cm^{-1}): 2925, 2854 (m, $\tilde{\nu}$ (C_{al}-H)); 2194 (s, ν_{as}(C≡N)); 1591, 1566 (m, ν (C_{ar}-C_{ar}) and ν(C_{ar}-N_{ar})); 1483, 1459, 1433, 1330, 752 (s, $\tilde{\nu}$ (CH)); 613, 430. UV-VIS (acetonitrile, λ/nm): 313 (π→π*), 343 (n→π*).

Complex **3** $[Co(L2)_2][Co(NCO)_4]$: Yield 37% (258 mg, 0.19 mmol). Elemental analysis for $C_{74}H_{90}Co_2N_{14}O_4$ (M_w = 1357.45g mol^{-1}) found % (expected %): C 65.74 (65.47); N 13.76 (14.45); H 6.27 (6.68). FT−IR (ATR, ν_{max}/cm^{-1}): 2925, 2851 (m, ν (C_{al}-H)); 2207 shoulder, 2188 (s, ν_{as}(C≡N)); 1598, 1567 (m, ν(C_{ar}-C_{ar}) and ν(C_{ar}-N_{ar})); 1498, 1433, 1329, 743 (s, δ(CH)); 611, 427. UV-VIS (acetonitrile, λ/nm): 313 (π→π*), 343 (n→π*).

Complex **4** $[Co(L3)_2][Co(NCO)_4]\cdot 2CH_3CN$: Yield 39% (158 mg, 0.19 mmol). Elemental analysis for $C_{94}H_{128}Co_2N_{16}O_4$ (M_w = 1663.99g mol^{-1}) found % (expected %): C 68.67 (68.33); N 13.12 (12.40); H 8.09 (7.77). FT−IR (ATR, ν_{max}/cm^{-1}): 2922, 2851 (m, ν(C_{al}-H)); 2200shoulder, 2190 (s, ν_{as}(C≡N)); 1597, 1569 (m, ν(C_{ar}-C_{ar}) and ν(C_{ar}-N_{ar})); 1480, 1435, 1328, 743 (s, δ(CH)); 612, 429. UV-VIS (acetonitrile, λ/nm): 313 (π→π*), 343 (n→π*).

*Complex **2** $[Co(L1)_2][Co(NCS)_4]\cdot 0.5CH_3CN$*

An acetonitrile solution (10 ml) of $Co(NCS)_2$ (88 mg, 0.5 mmol, 1 eq.) was added into the acetonitrile solution (20 ml) of ligand **L1** (239 mg, 0.5 mmol, 1 eq.). The mixture obtained was refluxed for 45 minutes, filtered, and the resulting solution was allowed to undergo controlled crystallization at room temperature. Green block crystals suitable for X-ray diffraction were collected after a few days. Yield 31% (558 mg, 0.21 mmol). Elemental analysis for $C_{134}H_{150.53}Co_4N_{29}S_8$ (M_w = 2659.57 g mol^{-1}) found % (expected %): C 59.49 (60.53); N 14.39 (14.97); H 5.53 (5.70). FT−IR (ATR, intense peaks, $\tilde{\nu}_{max}$/cm^{-1}): 2925, 2854 (m, ν(C_{al}-H)); 2099, 2063 (s, ν_{as}(C≡N)); 1595, 1567 (m, ν(C_{ar}-C_{ar}) or ν (C_{ar}-N_{ar})); 1478, 1329, 751 (s, ν(CH)); 476, 423. UV-VIS (acetonitrile, λ/nm): 313 (π→π*), 341 (n→π*).

S 2.3 Computational details

The fitting of the magnetic susceptibility and magnetization of all compounds was performed with the program PHI 3.1.3[11]. Calculations of magnetic parameters were carried out within the program ORCA 4.2.0.[14] The ZFS parameters and crystal-field terms energies were obtained using the state averaged complete active space self-consistent field method[15] (SA-CAS[7,5]SCF) complemented by strongly-contracted N-electron valence perturbation theory of second-order (NEVPT2).[16] In either case 10 spin quartet states and 40 spin doublet reference states were taken into account. The resolution of identity for Coulomb interaction and the chain of spheres approximation for exchange integrals (RIJCOSX)[17] were set on for the construction of Fock matrices while sole resolution of identity was used in the CASSCF and NEVPT2 calculations. For all atoms the Ahlrichs' basis def2-TZVP[18] was used with auxiliary basis sets def2/J[19] and def2-TZVP/C[20]. Prior to this calculation, the positions of all hydrogen atoms were optimized on the model fragments using the method PBEh-3c[21] and all other atoms were kept in their positions as obtained from the X-ray analysis. The ZFS parameters were calculated by quasi-degenerate perturbation theory (QDPT),[22,23] in which an approximation to the Breit-Pauli form of the spin-orbit coupling operator (SOMF approximation)[23] and the effective Hamiltonian theory were utilized.[24] The predicted curves were constructed based on the detailed ORCA output using a home-made MATLAB code.[25]

S 2.4 Crystallography

Data collection and cell refinement of **3** and **4** were made using a Stoe StadiVari (Stoe & Cie GmbH, Darmstadt, Germany) diffractometer using a Pilatus3R 300K hybrid pixel array detector and microfocused X-ray source Xenocs Genix3D Cu HF (Cu Kα radiation). For compounds **1** and **2**, data

collection was done using an XtaLAB Synergy-I diffractometer with a HyPix3000 hybrid pixel array detector and microfocused PhotonJet-I X-ray source (Cu Kα). All crystal structures were solved using a ShelXT program[26] and refined by the full matrix least-squares procedure using Olex2.refine and ShelXL[27] in OLEX2 (version 1.5).[28] The multi-scan absorption corrections were applied using the program Stoe LANA software[29] or CrysAlisPro 1.171.40.82a.[30] Crystal structure refinement: all non-hydrogen atoms were refined anisotropically. The hydrogen atoms were placed at the calculated positions and they were included in the riding-model approximation with U_{iso} = 1.2U_{eq}(C) or 1.5U_{eq}(CH3) and d(C–H) = 0.95–0.98 Å.

S2 Spectral characterization of prepared compounds

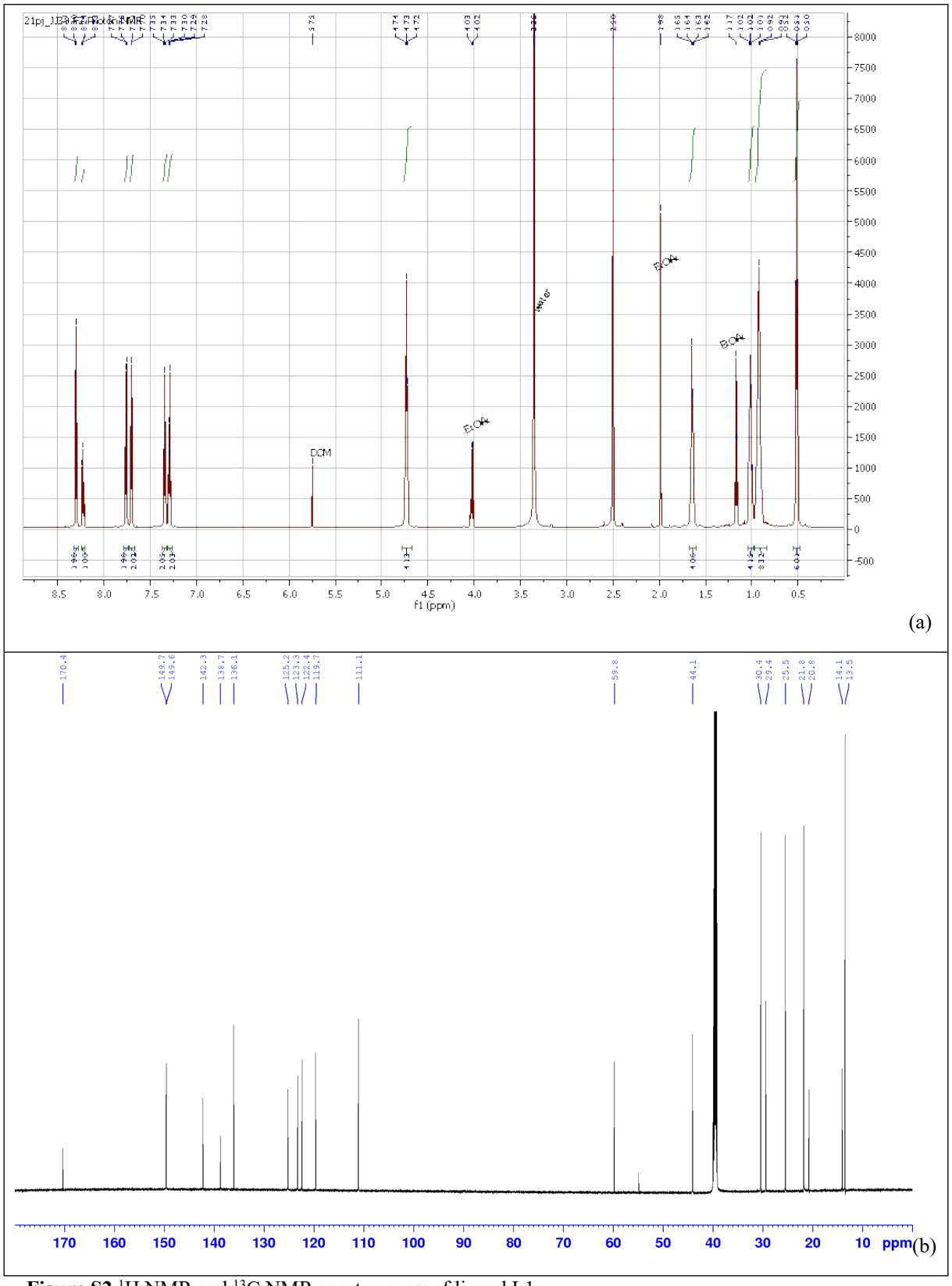

Figure S2 ^{1}H NMR and ^{13}C NMR spectroscopy of ligand L1

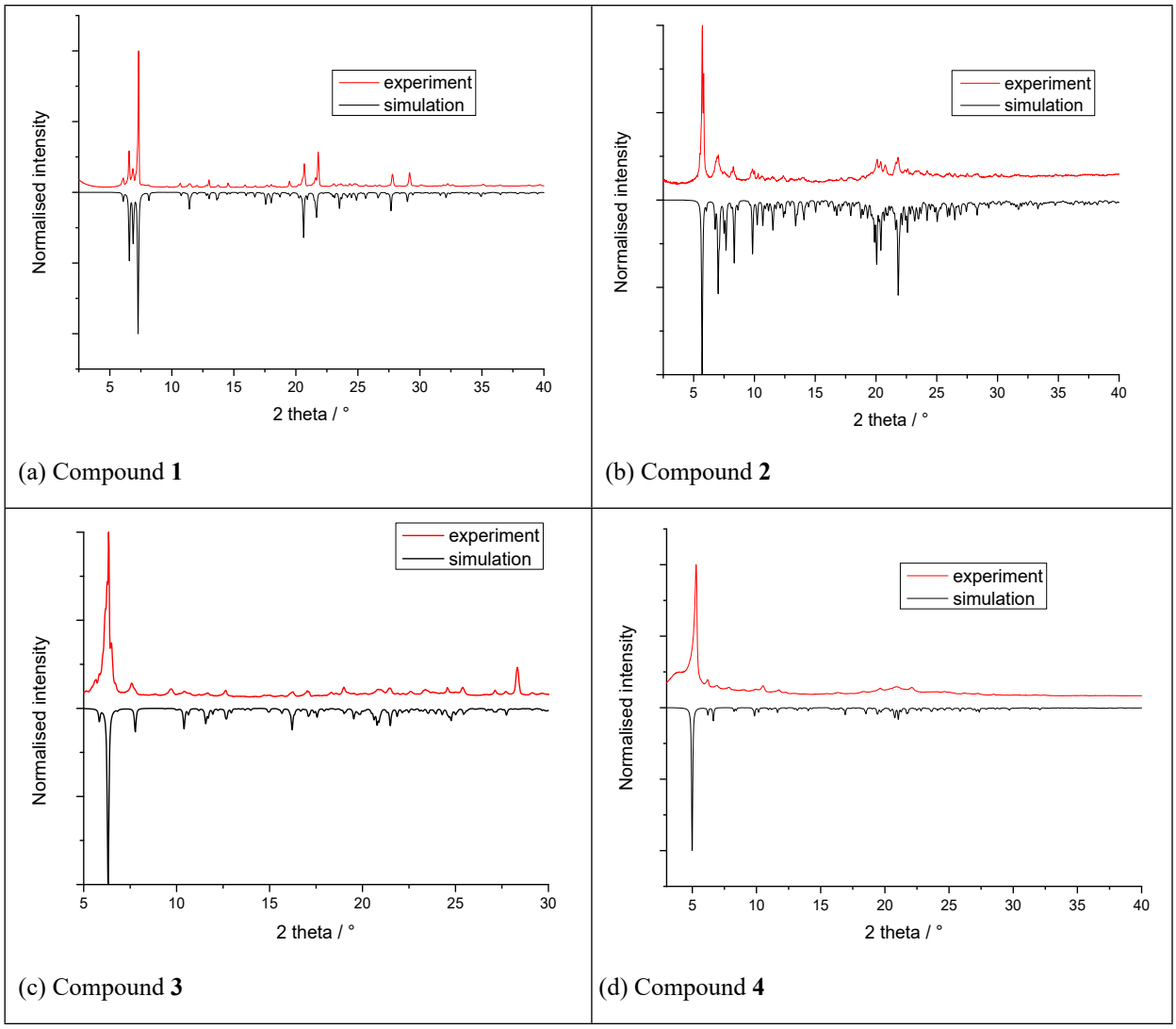

Figure S3 X-ray powder diffractogram of **1**-**4**.

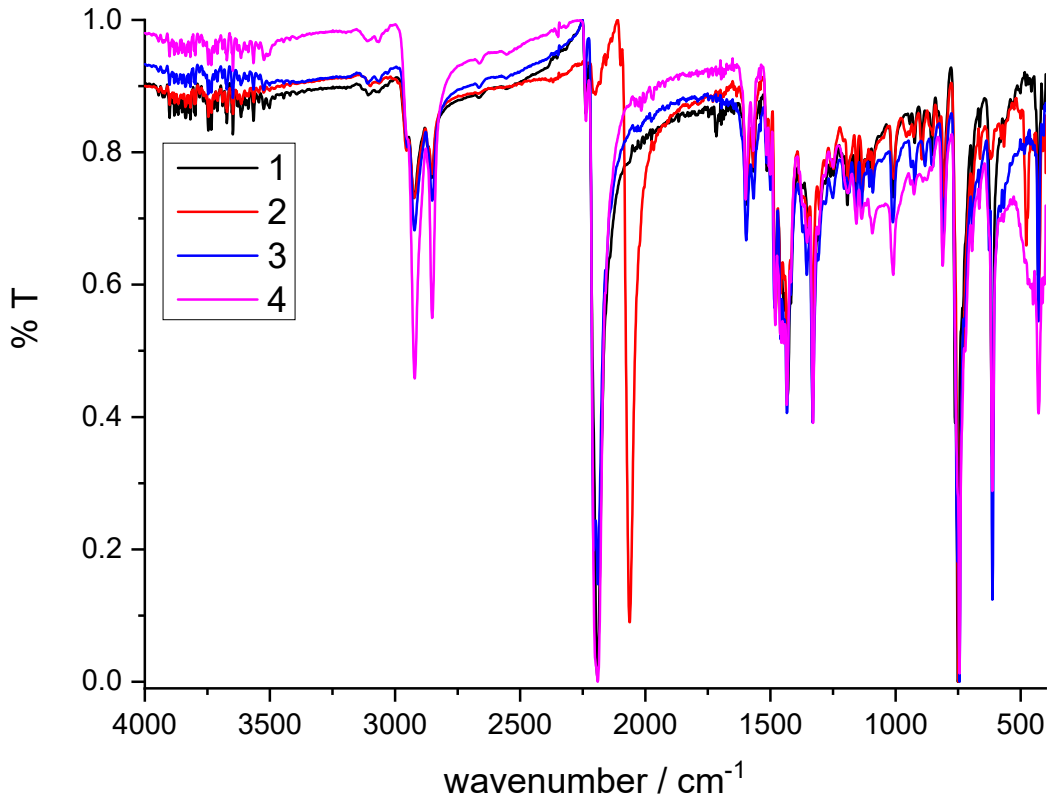

Figure S4 FT-IR spectra of **1**-**4**.

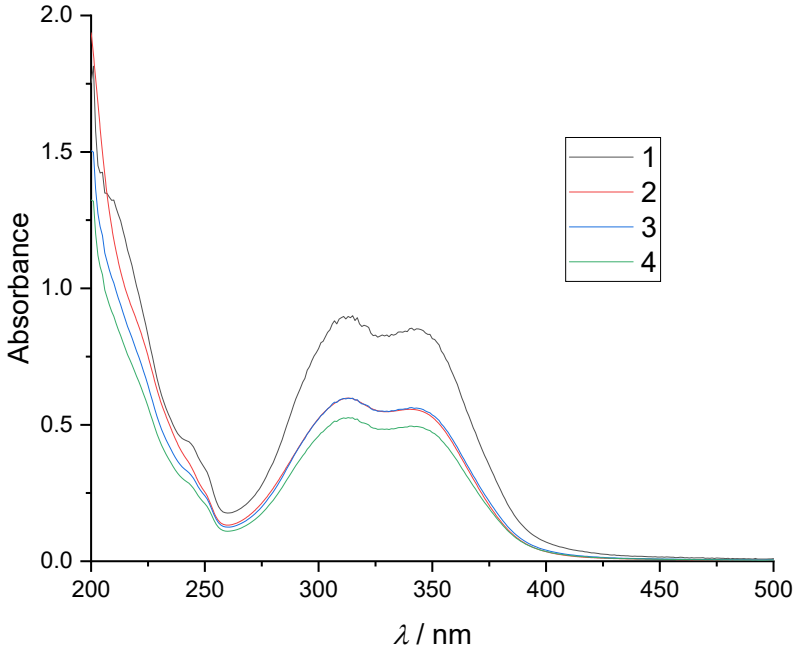

Figure S5 UV-VIS spectra of **1**-**4** recorded in acetonitrile solution.

S3 Structural information

Table S2 Selected crystallographic information for reported complexes **1**-**4**.

	1	**2**	**3**	**4**
Formula	$C_{66}H_{74}Co_2N_{14}O_4$	$C_{134}H_{150.53}Co_4N_{29}S_8$	$C_{74}H_{90}Co_2N_{14}O_4$	$C_{94}H_{128}Co_2N_{16}O_4$
M_w / g mol^{-1}	1245.25	1329.78	1357.45	1663.98
T / K	293(1)	100(1)	293(1)	100(1)
λ / Å	1.54184	1.54184	1.54186	1.54186
Crystal system	triclinic	triclinic	triclinic	monoclinic
Space group	*P*-1	*P*-1	*P*-1	$P2_1/c$
a/Å	15.6926(7)	13.85829(6)	15.3479(4)	19.8535(6)
b/Å	15.7264(6)	16.47082(7)	17.0718(5)	27.2121(5)
c/Å	16.0729(8)	31.54082(12)	17.0508(5)	18.7151(4)
α/°	109.687(4)	78.9901(4)	64.451(2)	90
β/°	90.185(4)	80.0612(3)	89.478(2)	113.315(3)
γ/°	117.019(4)	69.1223(4)	67.694(2)	90
Volume/Å^3	3268.9(3)	6559.89(5)	3664.61(19)	9285.3(4)
Z; ρ_{calc}/g·cm^{-3}	2; 1.265	2; 1.346	2; 1.230	4; 1.190
μ/mm^{-1}	4.431	5.565	3.992	3.245
F(000)	1308.0	2787.0	1436	3560.0
Final *R*indices [$I>2\sigma(I)$][a]	R_1 = 0.0629, wR_2 = 0.1822	R_1 = 0.0396, wR_2 = 0.1086	R_1 = 0.0636, wR_2 = 0.1480	R_1 = 0.1086, wR_2 = 0.2926
R indices (all data)[a]	R_1 = 0.0849, wR_2 = 0.2009	R_1 = 0.0417, wR_2 = 0.1097	R_1 = 0.1071, wR_2 = 0.1761	R_1 = 0.1267, wR_2 = 0.3057
GoF on F^2	1.074	1.087	1.067	1.052
CCDC no.	2352529	2352530	2352531	2352532

[a] $R1 = \sum(F_0 - F_C)/\sum(F_0)$; $wR2 = \sqrt{\sum[w(F_0^2 - F_C^2)^2]/\sum[w(F_0^2)^2]}$

Table S3 Bond distances of coordination polyhedra in reported compounds

	$[Co(L1)_2]^{2+}$ of **1**	$[Co(L1)_2]^{2+}$ of **2**		$[Co(L2)_2]^{2+}$ of **3**	$[Co(L3)_2]^{2+}$ of **4**
		Co1A	Co1B		
Co1-N1 / Å	2.111(2)	2.1281(15)	2.106(2)	2.125(3)	2.119(5)
Co1-N2 / Å	2.109(3)	2.0829(15)	2.137(2)	2.100(3)	2.094(5)
Co1-N3 / Å	2.120(3)	2.1014(15)	2.116(1)	2.109(3)	2.138(5)
Co1-N4 / Å	2.124(3)	2.1155(15)	2.160(2)	2.126(3)	2.106(4)
Co1-N5 / Å	2.108(2)	2.0870(15)	2.113(1)	2.099(3)	2.087(5)
Co1-N6 / Å	2.160(3)	2.1116(15)	2.156(2)	2.139(3)	2.113(5)
	$[Co(NCO)_4]^{2-}$ of **1**	$[Co(NCS)_4]^{2-}$ of **2**		$[Co(NCO)_4]^{2-}$ of **3**	$[Co(NCO)_4]^{2-}$ of **4**
		Co1A	Co1B		
Co2-N7 / Å	1.942(4)	1.9753(18)	1.946(2)	1.970(4)	1.950(7)
Co2-N8 / Å	1.961(6)	1.9549(18)	1.965(2)	1.944(4)	1.977(7)
Co2-N9 / Å	1.942(4)	1.9585(18)	1.964(2)	1.937(4)	1.977(6)
Co2-N10 / Å	1.967(5)	1.9587(18)	1.957(2)	1.966(6)	1.954(6)

Table S4 Angles of coordination polyhedra and miscellaneous structural parameters of coordination polyhedra calculated for the reported compounds.

angles	$[Co(L1)_2]^{2+}$ of **1**/°	$[Co(L1)_2]^{2+}$ of **2**/°		$[Co(L2)_2]^{2+}$ of **3**/°	$[Co(L3)_2]^{2+}$ of **4**/°
		Co1A	Co1B		
N2-Co1-N4	114.07(10)	100.09(6)	106.72(6)	112.47(12)	104.98(17)
N2-Co1-N6	95.04(10)	107.91(6)	103.90(6)	96.13(12)	102.99(18)
N2-Co1-N1	75.31(10)	76.03(6)	75.23(6)	75.66(12)	76.03(18)
N2-Co1-N3	75.92(10)	76.21(6)	75.60(6)	75.74(11)	76.26(18)
N1-Co1-N4	87.99(10)	88.91(6)	88.37(6)	95.67(12)	90.09(18)
N3-Co1-N4	95.87(11)	99.10(6)	100.02(6)	91.10(11)	96.35(18)
N1-Co1-N6	100.23(10)	98.48(6)	93.87(6)	89.05(13)	92.75(19)
N3-Co1-N6	90.79(11)	86.95(6)	93.03(6)	98.36(12)	94.11(19)
N5-Co1-N1	112.11(10)	97.92(6)	110.31(6)	100.15(12)	107.57(18)
N5-Co1-N3	97.66(10)	109.98(6)	98.85(6)	108.79(11)	100.15(19)
N5-Co1-N4	75.27(10)	76.32(6)	75.69(6)	75.52(12)	75.94(17)
N5-Co1-N6	75.77(10)	75.91(6)	74.39(6)	75.80(12)	76.40(17)
Σ / °	136	133	137	131	124
HP-6[a]	31.598	31.475	32.209	32.361	33.907
PPY-6[a]	17.191	19.140	18.719	18.823	20.133
OC-6[a]	4.940	4.253	4.747	4.460	4.005
TPR-6[a]	9.013	10.543	9.932	10.255	10.643
JPPY-6[a]	20.697	22.812	22.612	22.432	24.036
	$[Co(NCO)_4]^{2-}$of **1**/°	$[Co(NCS)_4]^{2-}$ of **2**/°		$[Co(NCO)_4]^{2-}$of **3**/°	$[Co(NCO)_4]^{2-}$ of **4**/°
		Co2A	Co2B		
N8-Co2-N7	110.2(3)	113.05(7)	105.10(8)	105.36(17)	110.3(3)
N8-Co2-N10	109.7(2)	113.98(8)	105.86(8)	110.9(2)	111.2(3)
N9-Co2-N7	112.8(2)	109.27(7)	105.77(8)	110.45(17)	111.4(2)
N9-Co2-N8	107.8(2)	110.25(7)	113.45(8)	112.96(19)	106.9(3)
N9-Co2-N10	107.55(18)	107.03(7)	106.40(8)	109.4(2)	109.4(2)
N10-Co2-N7	108.8(2)	102.86(8)	120.55(8)	107.53(19)	107.7(3)
τ_4	0.97	0.94	0.89	0.97	0.97
SP-4[b]	32.10	31.56	27.34	32.30	31.86
T-4[b]	0.03	0.16	0.47	0.06	0.04
SS-4[b]	9.05	8.61	6.72	9.02	9.17
vTBPY-4[b]	3.42	3.15	3.54	3.09	3.55

[a] Results of the SHAPE calculations for hexacoordinated polyhedra of hexagon (HP), pentagonal pyramid (PPY), octahedron (OC), trigonal prism (TPR), Johnson pentagonal pyramid (JPPY)

[b] Symmetry measure parameters for square (SP-4), tetrahedron (T-4), seesaw (SS-4), vacant trigonal bipyramid (vTBPY-4)

S4 Static Magnetic Properties

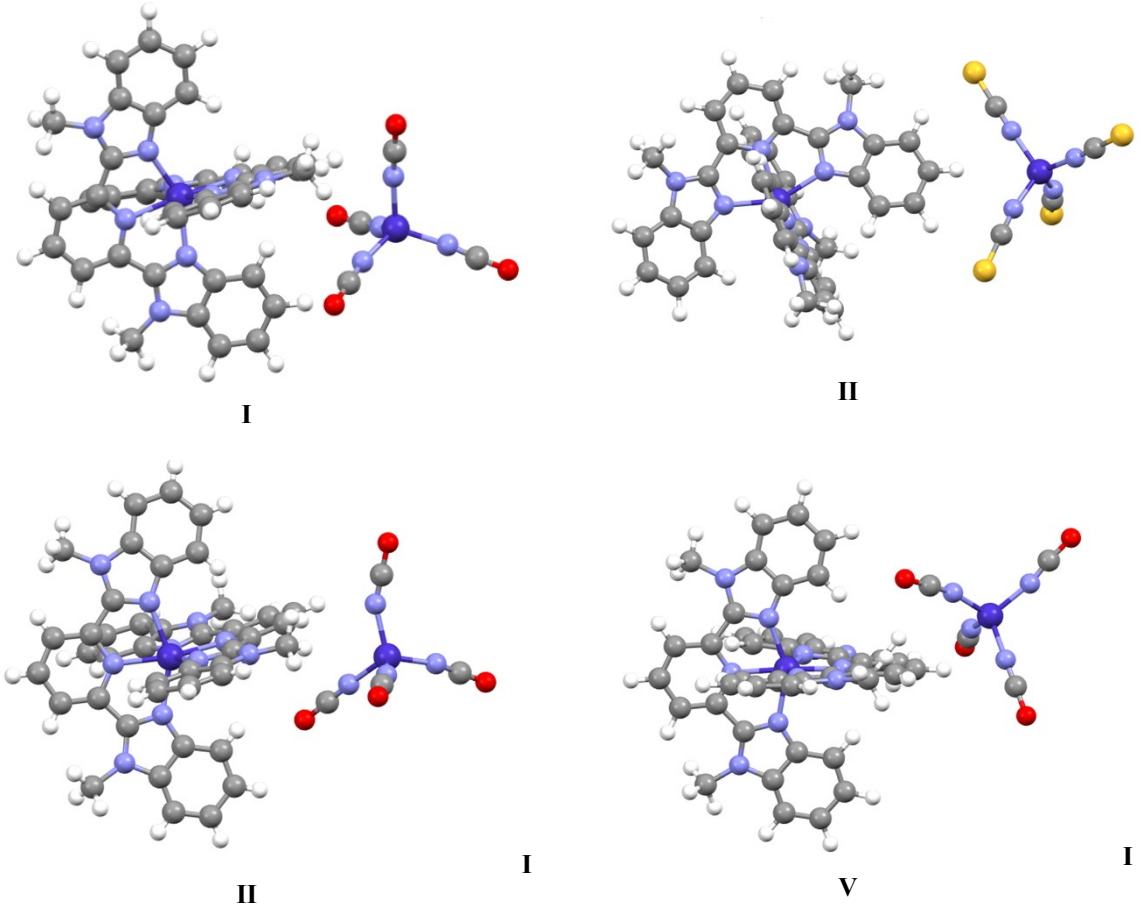

Figure S6 Geometries of model systems **I-IV** which were constructed by cutting the pendant aliphatic chains from moieties with octahedrally coordinated Co(II) centres (left part of each picture, called $\mathbf{I_{oct}}$-$\mathbf{IV_{oct}}$ in the text).

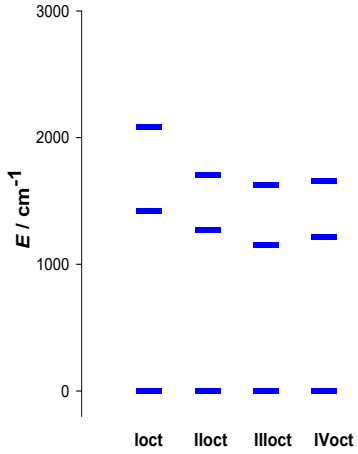

Figure S7 Energy of lowest spin-quartet eigenvalues from *ab-initio* calculations for model systems **Ioct-IVoct**.

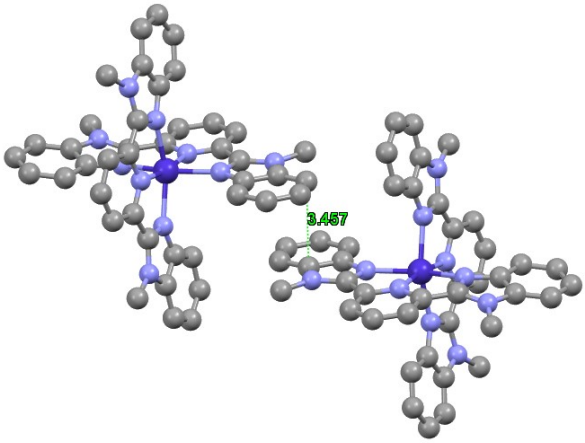

Figure S8 Dimer of octahedral sites in **III** investigated for assessment of exchange interaction.

Table S5 Broken-Symmetry DFT assessment of magnetic exchange interaction in dimer of octahedral sites in **III**.

	PBE0 / def2-TZVP	**B3LYP / def2-TZVP**
J /cm^{-1}	−0.86	−0.12

S5 FIRMS

Fourier-transform infrared magnetic spectroscopy (FIRMS) was carried out at the National Laboratory for Intense Magnetic Fields (LNCMI) of the French National Center for Scientific Research (CNRS) to determine the magneto-optical response of the studied compounds in the THz range and a direct observation of the ZFS parameters. The experiments were conducted in transmission mode using a Bruker Vertex 80v Fourier-transform spectrometer coupled with a 16 T superconducting magnet in a Faraday configuration, i.e., with unpolarized light and the magnetic field parallel to the wave vector of the probing radiation. We used a globar as radiation source that was delivered through light-pipe optics to the pellet-pressed samples situated inside the superconducting coil, maintained in helium heat-exchange gas at T = 4.2 K. After passing through the pellet, the radiation was detected using a composite silicon bolometer (Infrared Laboratories, Tuscon, USA) placed just below it. The pellets were prepared by combining the compounds with 90% *n*-eicosane, ensuring transparency in the spectral range of our interest.

The FIRMS transmission spectra were measured from 0 to 1000 cm^{-1} with 2 cm^{-1} resolution and normalized by the average of all spectra to remove field-independent features, enabling identification of magnetic absorptions. When indicated in the text, the colormaps are made from the derivative of the resulting spectra to aid the identification of the field-dependent signals (magnetic absorptions). For most samples, the sensitivity of our experiments is sufficient for observation of at least one feature that shifts with the applied magnetic field, allowing extrapolation of the magnetic absorption signals at zero magnetic field. Since the experiments were performed with polycrystalline (finely ground powder) samples prepared as diluted pellets with *n*-eicosane, relatively broad spectra lack details beyond the signal-to-noise ratio (SNR) due to the available power from our light source. Therefore, a precise fitting allowing determination of the g matrix and rhombicity (E/D) is not straightforward (or even possible). As a workaround, we used these parameters from other methods such as ab initio calculations to aid the simulation and quantification of the ZFS parameters $|D|$.

The simulations shown on the top of the FIRMS data were performed using EasySpin[26] and the vibronic coupling model described in reference[27] using MATLAB.[25]

S6 Dynamic magnetic investigation

The magnetic data induced by the oscillating; AC magnetic field were obtained at an amplitude of B_{AC} = 0.5 mT. In order to determine the optimum DC field for suppressing the quantum tunnelling of magnetization, AC susceptibility measurements under various DC fields were applied at 2 K. Collected sets of χ' and χ'' at each temperature were fitted using the formulas for extended one-set Debye model (equations S1, S2) or extended two-set Debye model (equations S3, S4).

$$\chi'(\omega) = \chi_S + (\chi_T - \chi_S)\frac{1+(\omega\tau)^{(1-\alpha)}\sin(\pi\alpha/2)}{1+2(\omega\tau)^{(1-\alpha)}\sin(\pi\alpha/2)+(\omega\tau)^{(2-2\alpha)}} \quad \textbf{(S1)}$$

$$\chi''(\omega) = (\chi_T - \chi_S)\frac{(\omega\tau)^{(1-\alpha)}\cos(\pi\alpha/2)}{1+2(\omega\tau)^{(1-\alpha)}\sin(\pi\alpha/2)+(\omega\tau)^{(2-2\alpha)}} \quad \textbf{(S2)}$$

$$\chi'(\omega) = \chi_S + (\chi_{T1} - \chi_S)\frac{1+(\omega\tau_1)^{(1-\alpha_1)}\sin(\pi\alpha_1/2)}{1+2(\omega\tau_1)^{(1-\alpha_1)}\sin(\pi\alpha_1/2)+(\omega\tau_1)^{(2-2\alpha_1)}} + (\chi_{T2} - \chi_{T1})\frac{1+(\omega\tau_2)^{(1-\alpha_2)}\sin(\pi\alpha_2/2)}{1+2(\omega\tau_2)^{(1-\alpha_2)}\sin(\pi\alpha_2/2)+(\omega\tau_2)^{(2-2\alpha_2)}} \quad \textbf{(S3)}$$

$$\chi''(\omega) = (\chi_{T1} - \chi_S)\frac{(\omega\tau_1)^{(1-\alpha_1)}\cos(\pi\alpha_1/2)}{1+2(\omega\tau_1)^{(1-\alpha_1)}\sin(\pi\alpha_1/2)+(\omega\tau_1)^{(2-2\alpha_1)}} + (\chi_{T2} - \chi_{T1})\frac{(\omega\tau_2)^{(1-\alpha_2)}\cos(\pi\alpha_2/2)}{1+2(\omega\tau_2)^{(1-\alpha_2)}\sin(\pi\alpha_2/2)+(\omega\tau_2)^{(2-2\alpha_2)}} \quad \textbf{(S4)}$$

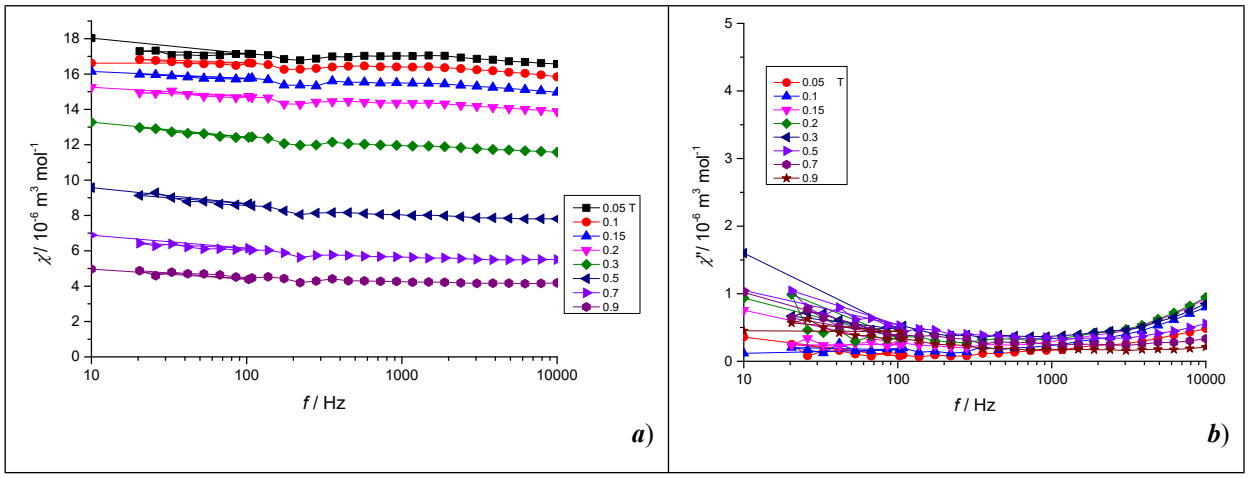

Figure S9 AC susceptibility data for **1** recorded at 2 K and at various static magnetic fields: Frequency dependent in-phase χ'(*a*) and out-of-phase χ''(*b*) component of AC susceptibility.

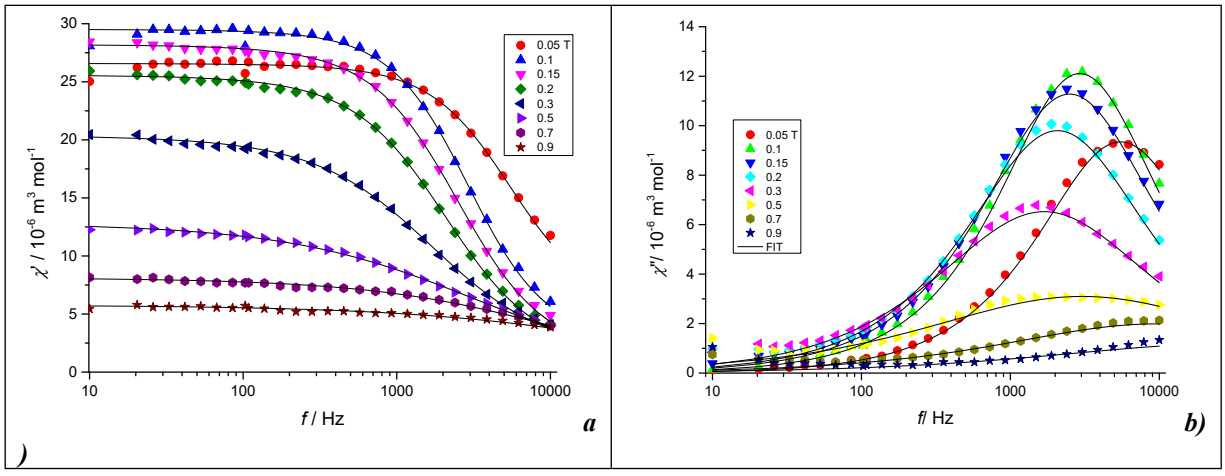

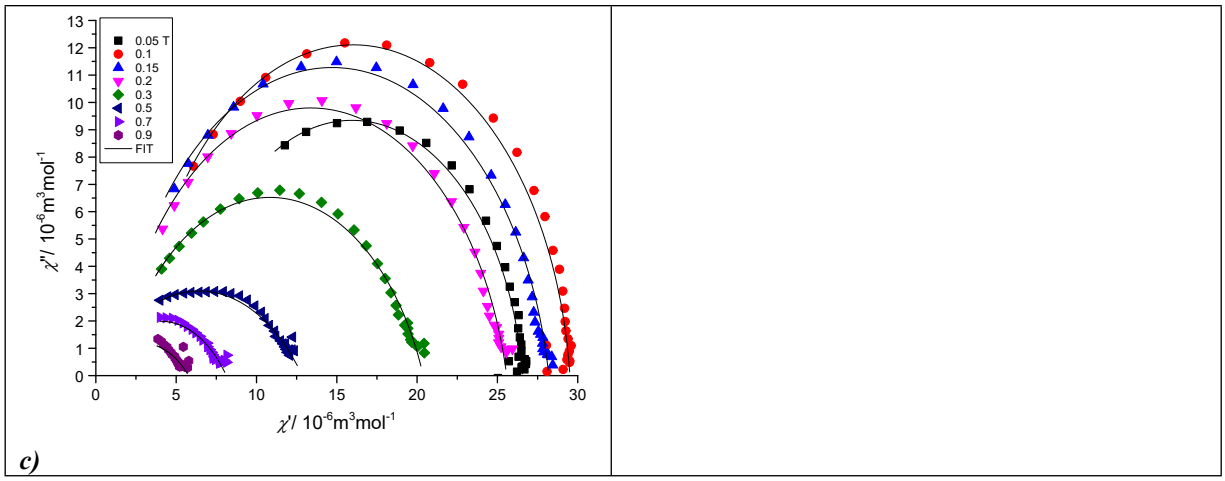

Figure S10 AC susceptibility data for **2** recorded at various static magnetic fields at T = 2.0 K: Frequency dependent in-phase χ'(a) and out-of-phase χ''(b) component of AC susceptibility and Cole-Cole diagram (c) (solid lines are results of fits according to equations S1 and S2).

Table S6 Parameters of the extended one-set Debye model (eq. S1 and S2) for **2** measured from 0 T to 0.9 T at T = 2.0 K.

B / T	χ_T/10^{-6} cm^3 mol^{-1}	χ_S /10^{-6} cm^3 mol^{-1}	α	τ /s	R^2
0.05	26.57(7)	5.3(4)	0.08(1)	2.90(9)×10^{-5}	0.9993
0.1	29.51(9)	2.5(3)	0.069(9)	5.44(9))×10^{-5}	0.99909
0.15	28.20(6)	1.2(2)	0.113(6)	6.36(7)×10^{-5}	0.99963
0.2	25.29(7)	1.2(2)	0.139(7)	7.7(1)×10^{-5}	0.99937
0.3	20.38(7)	1.3(2)	0.237(9)	9.4(2)×10^{-5}	0.99913
0.5	12.85(8)	0(0)	0.428(9)	5.2(2)×10^{-5}	0.998
0.7	8.12(6)	0(0)	0.42(1)	1.66(7)×10^{-5}	0.99756
0.9	5.77(8)	0(0)	0.50(4)	5.1(7)×10^{-6}	0.99335

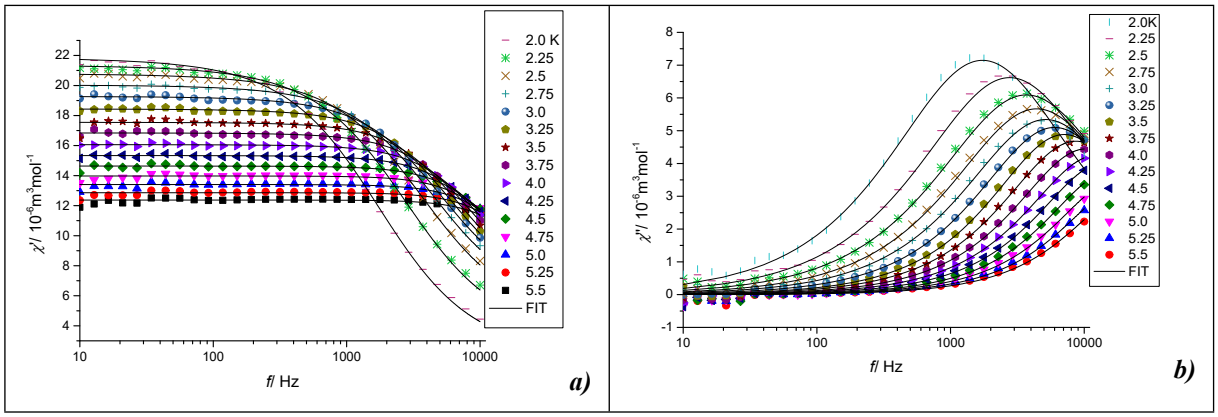

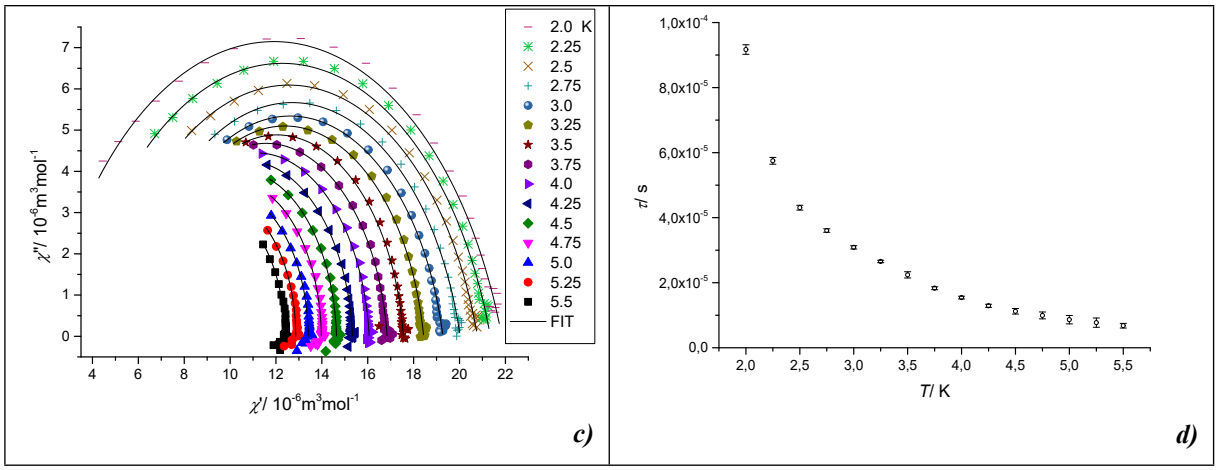

Figure S11 AC susceptibility data for **2** recorded in temperature range 2-5.5 K: Frequency dependent in-phase χ'(*a*) and out-of-phase χ''(*b*) component of AC susceptibility and Cole-Cole diagram (*c*) (solid lines are results of fits according to equations S1 and S2). Temperature dependence of the relaxation time (*d*).

Table S7 Parameters of the extended one-set Debye model (eq. S1 and S2) for **2** measured at 0.3 T.

T /K	χ_T /10^{-6} cm^3 mol^{-1}	χ_S /10^{-6} cm^3 mol^{-1}	α	τ / s	R^2
2.0	21.84(6)	2.0(1)	0.206(7)	9.2(2)×10^{-5}	0.99951
2.25	21.35(4)	3.2(2)	0.198(7)	5.7(1)×10^{-5}	0.99967
2.5	20.78(3)	4.4(2)	0.187(6)	4.31(7)×10^{-5}	0.99981
2.75	20.03(2)	5.4(2)	0.161(5)	3.60(5)×10^{-5}	0.999
3.0	19.28(2)	6.0(1)	0.139(6)	3.09(5)×10^{-5}	0.999
3.25	18.44(2)	6.3(1)	0.108(5)	2.65(4)×10^{-5}	0.99994
3.5	17.55(4)	6.5(3)	0.08(2)	2.24(9)×10^{-5}	0.99956
3.75	16.84(2)	6.3(2)	0.076(8)	1.83(4)×10^{-5}	0.99991
4.0	16.06(1)	6.3(2)	0.060(8)	1.54(4)×10^{-5}	0.99993
4.25	15.34(1)	6.1(2)	0.050(9)	1.29(5)×10^{-5}	0.99992
4.5	14.64(2)	6.2(5)	0.03(2)	1.12(9)×10^{-5}	0.99978
4.75	13.98(2)	6.3(6)	0.01(2)	1.0(1)×10^{-5}	0.99973
5.0	13.41(3)	6.2(8)	0.01(3)	0.9(1)×10^{-5}	0.99968
5.25	12.86(2)	6.2(9)	0.00(3)	0.8(1)×10^{-5}	0.99968
5.5	12.37(2)	6.0(6)	0(0)	0.68(7)×10^{-5}	0.99962

Table S8 Relaxation parameters at B_{DC} = 0.3 T for compound **2** using the respective combinations of Orbach. Raman and Direct processes of relaxation

Model	U_{eff}/k_B / K	τ_0/s	C / K^{-n} s^{-1}; n	AB^m / K^{-1} s^{-1}	R^2
Orbach for 4.5 - 5.5 K	12.4(4)	7.2(6)×10^{-7}	-	-	0.99521
Orbach&Raman*	6.8(3)	3.0(3)×10^{-6}	0.013(2); 9	-	0.99343
Orbach&Raman	42(97)	1(8)×10^{-7}	2325(306); 2.4(1)	-	0.99437
Orbach&direct	13(1)	9(2)×10^{-7}		5301(657)	0.99033
Raman&direct	-	-	2215(140); 2.45(5)	1(127)×10^{-9}	0.99044
Orbach&Raman&direct*	**8(1)**	**2.4(6)×10^{-6}**	**1.0(0.3)×10^{-2}; 9**	**2800(1503)**	**0.99377**

Orbach&Raman&direct	14(3)	$1.0(7)\times10^{-6}$	3746(3817); 2(2)	5.5×10^{-9}	0.99044
Orbach&direct&phonons*	**10.3(9)**	**$1.6(3)\times10^{-6}$**	**-**	**4116(815)**	**0.9939**

*Raman exponent has been fixed to n=9

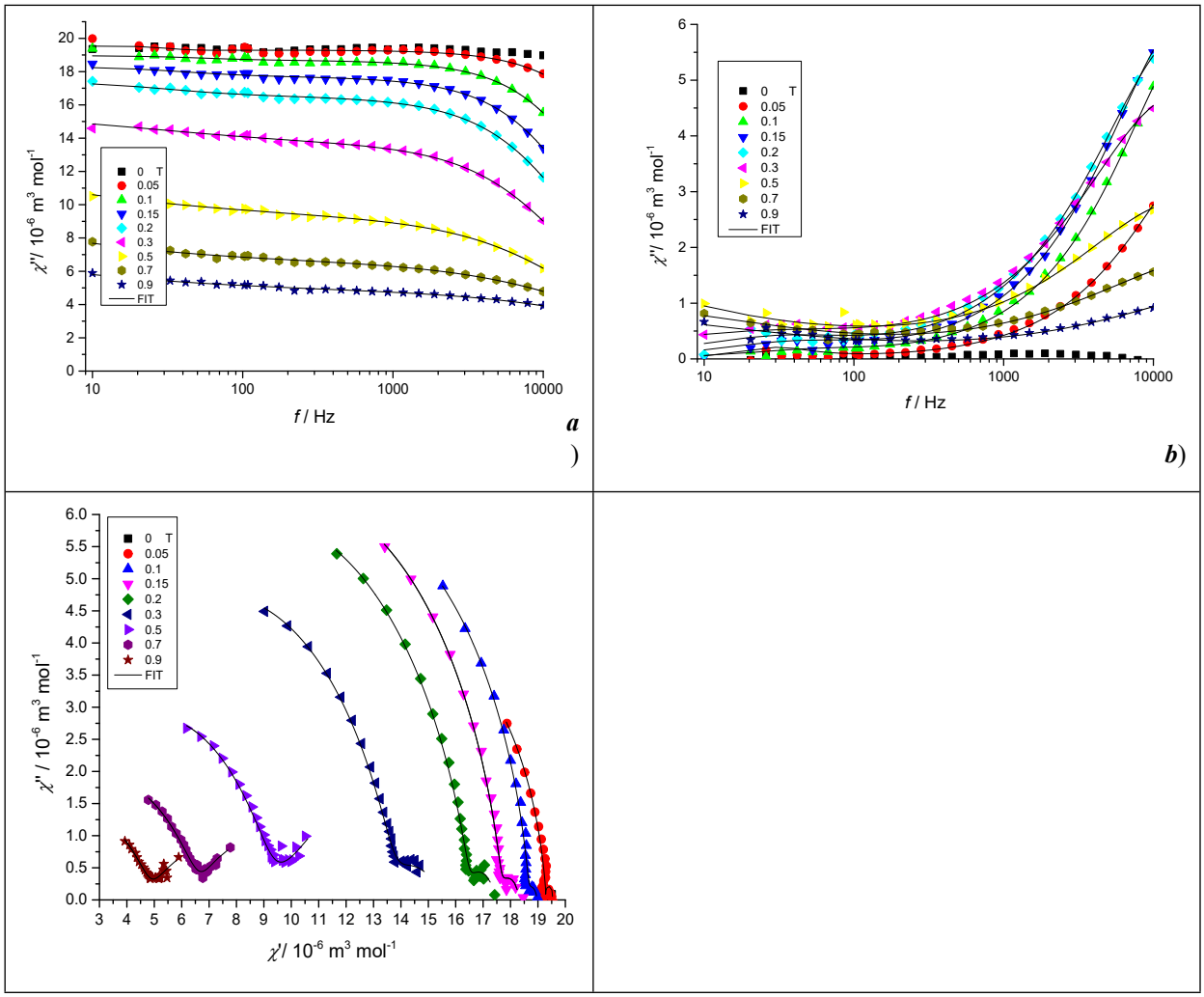

Figure S12 AC susceptibility measurement for **3** recorded at 2 K and at various DC magnetic fields: Frequency dependent in-phase χ'(*a*) and out-of-phase χ''(*b*) component of AC susceptibility and Cole-Cole diagram (*c*) (solid lines are results of fits according to equations S3 and S4).

Table S9 Parameters of the extended two-set Debye model (eq. S3 and S4) for **3** measured from 0.05 T to 0.9 T at $T = 2.0$ K. The parameters of the subtle low-frequency relaxation channel were disregarded.

***B* / T**	**χ_T/10^{-6} cm^3 mol^{-1}**	**χ_S/10^{-6} cm^3 mol^{-1}**	**α**	**τ /s**	**R^2**
0.05	19.31(3)	10(2)	0.09(4)	$5(1)\times10^{-6}$	0.99985
0.1	18.96(7)	4(1)	0.10(2)	$7.1(9)\times10^{-5}$	0.99984
0.15	18.30(8)	2.4(6)	0.12(1)	$8.4(6)\times10^{-6}$	0.99963
0.2	17.4(1)	1.4(6)	0.16(1)	$9.2(6)\times10^{-6}$	0.99989
0.3	15.4(3)	1.1(6)	0.19(2)	$1.06(8)\times10^{-5}$	0.99987
0.5	-	0(0)	0.25(3)	$9(2)\times10^{-6}$	0.99976
0.7	11(2)	0(0)	0.35(1)	$5(2)\times10^{-6}$	0.99964
0.9	9(3)	0(0)	0.37(4)	$5.1(7)\times10^{-6}$	0.99947

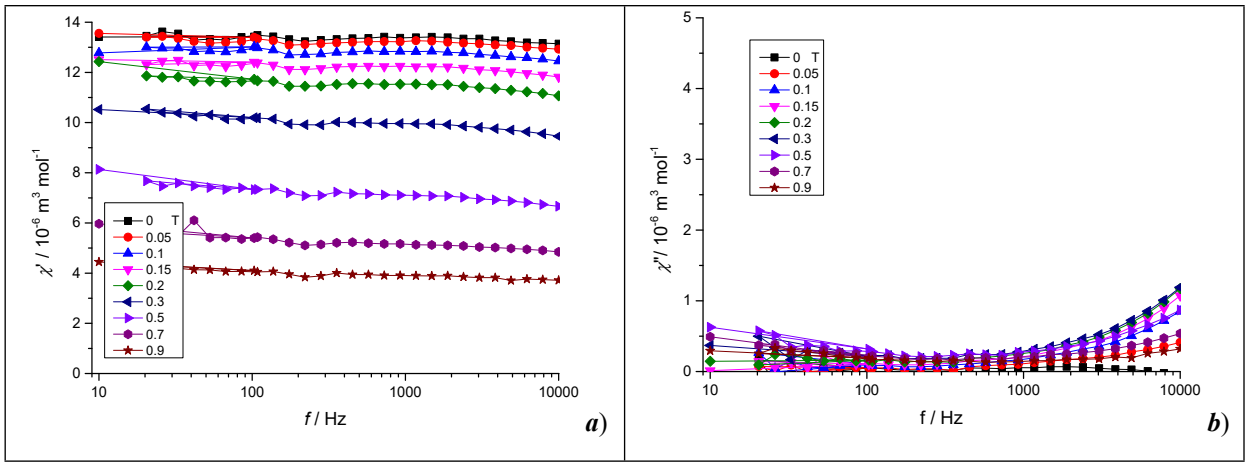

Figure S13 AC susceptibility data for **4** recorded at 2 K and at various static magnetic fields: Frequency dependent in-phase χ'(*a*) and out-of-phase χ''(*b*) component of AC susceptibility.

References

1. S. Ghosh, S. Kamilya, M. Das, S. Mehta, M.-E. Boulon, I. Nemec, M. Rouzières, R. Herchel, A. Mondal, Impact of Counteranion on Reversible Spin-State Switching in a Series of Cobalt(II) Complexes Containing a Redox-Active Ethylenedioxythiophene-Based Terpyridine Ligand, *Inorg. Chem*. 2020, **59**, 7067 – 7081.
2. K. Choroba, J. Palion-Gazda, B. Machura, A. Bieńko, D. Wojtala, D. Bieńko, C. Rajnák, R. Boča, A. Ozarowski, M. Ozerov, Large Magnetic Anisotropy in Mono- and Binuclear cobalt(II) Complexes: The Role of the Distortion of the Coordination Sphere in Validity of the Spin-Hamiltonian Formalism, *Inorg. Chem*. 2024, **63**, 1068–1082.
3. D. Shao, L. D. Deng, L. Shi, D. Q. Wu, X. Q. Wei, S. R. Yang and X. Y. Wang, Slow Magnetic Relaxation and Spin-Crossover Behavior in a Bicomponent Ion-Pair Cobalt(II) Complex, *Eur J Inorg Chem*, 2017, **2017**, 3862–3867.
4. Y. Zhang, K. L. M. Harriman, G. Brunet, A. Pialat, B. Gabidullin, M. Murugesu, Reversible Redox, Spin Crossover, and Superexchange Coupling in 3d Transition-Metal Complexes of Bis-azinyl Analogues of 2,2′:6′,2″-Terpyridine, *Eur. J. Inorg. Chem*. 2018, 1212–1223.
5. A. Galet, A. B. Gaspar, M. Carmen Munoz, J. A. Real, Influence of the Counterion and the Solvent Molecules in the Spin Crossover System [Co(4-terpyridone)$_2$]Xp.nH_2O *Inorg. Chem*. 2006, **45**, 4413−4422.
6. J. Palion-Gazda, B. Machura, R. Kruszynski, T. Grancha, N. Moliner, F. Lloret, M. Julve, Spin Crossover in Double Salts Containing Six- and Four-Coordinate Cobalt(II) Ions *Inorg. Chem.* 2017, **56**, 6281−6296.
7. S. S. Massoud, M. Dubin, A. E. Guilbeau, M. Spell, R. Vicente, P. Wilfling, R. C. Fischer, F. A. Mautner, Azido- and thiocyanato-cobalt(II) complexes based pyrazole ligands, *Polyhedron* 2014, **78**, 135–140.
8. Addison, A.W. and P.J. Burke, Synthesis of some imidazole- and pyrazole- derived chelating agents, *Journal of Heterocyclic Chemistry*, 1981, **18**, 803-805.
9. J. Juráková, J. Dubnická Midlíková, J. Hrubý, A. Kliuikov, V. T. Santana, J. Pavlik, J. Moncoľ, E. Čižmár, M. Orlita, I. Mohelský, P. Neugebauer, D. Gentili, M. Cavallini, I. Šalitroš, Pentacoordinate cobalt(ii) single ion magnets with pendant alkyl chains: shall we go for chloride or bromide? *Inorg. Chem. Front.*, 2022, **9**, 1179.
10. R. Boča. *Theoretical Foundations of Molecular Magnetism*. Elsevier. Amsterdam. 1999.
11. L. Banci, A. Bencini, C. Benelli, D. Gatteschi and C. Zanchini, *Structures versus Special Properties*, 1982, 37–86.
12. R. Boča, Zero-field splitting in metal complexes, *Coord. Chem. Rev.*, 2004, **248**, 757–815.
13. N. F. Chilton, R. P. Anderson, L. D. Turner, A. Soncini, K. S. Murray, N. F. Chilton, R. P. Anderson, L. D. Turner, A. Soncini, K. S. Murray, J. Comput. Chem., 2013, 34 (13), 1164-1175. *J. Comput. Chem.,* 2013, **34** (13), 1164-1175.
14. F. Neese, Software update: the ORCA program system, version 4.0. *WIREs Comput. Mol. Sci.* 2018, **8** (1), 1327.

15. P. A. Malmqvist, B. O. Roos, The CASSCF state interaction method, *Chem. Phys. Lett.* 1989, **155** (2), 189−194.
16. a) C. Angeli, R. Cimiraglia, J.-P. Malrieu, N-electron valence state perturbation theory: A fast implementation of the strongly contracted variant, *Chem. Phys. Lett.* 2001, **350**, 297−305; b) C. Angeli, R. Cimiraglia, S. Evangelisti, T. Leininger, J.-P. Malrieu, Introduction of n-electron valence states for multireference perturbation theory, *J. Chem. Phys.* 2001, **114**, 10252−10264; c) C. Angeli, R. Cimiraglia, J.-P. Malrieu, N-electron valence state perturbation theory: a spinless formulation and an efficient implementation of the strongly contracted and of the partially contracted variants, *J. Chem. Phys.* 2002, **117**, 9138−9153.
17. R. Izsak and F. Neese, An overlap fitted chain of spheres exchange method, *J. Chem. Phys.* 2011, **135**, 144105.
18. F. Weigend and R. Ahlrichs, Balanced basis sets of split valence, triple zeta valence and quadruple zeta valence quality for H to Rn: Design and assessment of accuracy, *Phys. Chem. Chem. Phys.* 2005, **7**, 3297-3305.
19. F. Weigend, Accurate Coulomb-fitting basis sets for H to Rn, *Phys. Chem. Chem. Phys.* 2006, **8**, 1057-1065.
20. A. Hellweg, C. Hattig, S. Hofener and W. Klopper, Optimized accurate auxiliary basis sets for RI-MP2 and RI-CC2 calculations for the atoms Rb to Rn, *Theor. Chem. Acc.* 2007, **117**, 587-597.
21. S. Grimme, J. G. Brandenburg, C. Bannwarth and A. Hansen, Consistent structures and interactions by density functional theory with small atomic orbital basis sets, *J. Chem. Phys.* 2015, **143**, 054107.
22. D. Ganyushin and F. Neese, First-principles calculations of zero-field splitting parameters , *J. Chem. Phys.* 2006, **125**, 024103.
23. F. Neese, Efficient and accurate approximations to the molecular spin-orbit coupling operator and their use in molecular-tensor calculations, *J. Chem. Phys.* 2005, **122**, 034107.
24. R. Maurice, R. Bastardis, C. de Graaf, N. Suaud, T. Mallah, N. Guihéry, Universal Theoretical Approach to Extract Anisotropic Spin Hamiltonians, *J. Chem. Theory Comput.* 2009, **5**, 2977–2984.
25. The MathWorks, Inc. MATLAB, 2023, version 9.14.0 (R2023a, Update 4).
26. G. M. Sheldrick, HELXT-Integrated Space-Group and Crystal-Structure Determination, *Acta Crystallogr., Sect. A: Found. Adv.*, 2015, 71, 3–8.
27. a) L. J. Bourhis, O. V. Dolomanov, R. Gildea, J. A. K. Howard and H. Puschmann, The anatomy of a comprehensive constrained, restrained refinement program for the modern computing environment - Olex2 dissected, Acta Crystallogr., Sect. A: Found. Adv., 2015, 71, 59–75; b) G. M. Sheldrick, Acta Crystallogr., *Sect. C: Struct. Chem.*, 2015, 71, 3–8.
28. O. Dolomanov, L. J. Bourhis, R. Gildea, J. A. Howard and H. Puschmann, A Complete Structure Solution, Refinement and Analysis Program, *J. Appl. Crystallogr*., 2009, 42, 339–341.
29. J. Koziskova, F. Hahn, J. Richter and J. Kožíšek, Comparison of different absorption corrections on the model structure of tetrakis(μ2-acetato)-diaqua-di-copper(II), *Acta Chim. Slovaca*, 2016, 9, 136–140.
30. CrysAlisPro 1.171.40.82a, Rigaku Oxford Diffraction, 2020
31. a) S. Stoll, A. Schweiger, EasySpin, a comprehensive software package for spectral simulation and analysis in EPR, *J. Magnet. Resonance*, 2006, **178**, 42-55; b) J. Nehrkorn, J. Telser, K. Holldack, S. Stoll and A. Schnegg, Simulating Frequency-Domain Electron Paramagnetic Resonance: Bridging the Gap between Experiment and Magnetic Parameters for High-Spin Transition-Metal Ion Complexes „*Journal of Physical Chemistry B*, 2015, **119**, 13816–13824.
32. D. H. Moseley, S. E. Stavretis, K. Thirunavukkuarasu, M. Ozerov, Y. Cheng, L. L. Daemen, J. Ludwig, Z. Lu, D. Smirnov, C. M. Brown, A. Pandey, A. J. Ramirez-Cuesta, A. C. Lamb, M. Atanasov, E. Bill, F. Neese and Z. L. Xue, Spin–phonon couplings in transition metal complexes with slow magnetic relaxation, *Nat. Commun. 2018 9:1*, 2018, **9**, 1–11.